Bioorganic & Medicinal Chemistry 18 (2010) 5738–5748

Contents lists available at ScienceDirect

Bioorganic & Medicinal Chemistry

journal homepage: www.elsevier.com/locate/bmc

The design, synthesis, and evaluation of 8 hybrid DFG-out allosteric kinase inhibitors: A structural analysis of the binding interactions of Gleevec®, Nexavar®, and BIRB-796

Justin Dietrich [a,d,*], Christopher Hulme [a,b,c,d], Laurence H. Hurley [a,b,c]

[a] Department of Pharmacology and Toxicology, College of Pharmacy, The University of Arizona, Tucson, AZ 85719, United States
[b] Arizona Cancer Center, University of Arizona, 1515 N. Campbell Avenue, Tucson, AZ 85724, United States
[c] BIO5 Institute, University of Arizona, 1657 E. Helen Street, Tucson, AZ 85721, United States
[d] Southwest Comprehensive Center for Drug Discovery and Development, College of Pharmacy, The University of Arizona, Tucson, AZ 85719, United States

ARTICLE INFO

Article history:
Received 26 March 2010
Revised 20 May 2010
Accepted 23 May 2010
Available online 4 June 2010

Keyword:
Allosteric structure based drug design
kinase type II

ABSTRACT

The majority of kinase inhibitors developed to date are competitive inhibitors that target the ATP binding site; however, recent crystal structures of Gleevec® (imatinib mesylate, STI571, PDB: 1IEP), Nexavar® (Sorafenib tosylate, BAY 43-9006, PDB: 1UWJ), and BIRB-796 (PDB: 1KV2) have revealed a secondary binding site adjacent to the ATP binding site known as the DFG-out allosteric binding site. The recent successes of Gleevec® and Nexavar® for the treatment of chronic myeloid leukemia and renal cell carcinoma has generated great interest in the development of other kinase inhibitors that target this secondary binding site. Here, we present a structural comparison of the important and similar interactions necessary for Gleevec®, Nexavar®, and BIRB-796 to bind to their respective DFG-out allosteric binding pockets and the selectivity of each with respect to c-Abl, B-Raf, and p38α. A structural analysis of their selectivity profiles has been generated from the synthesis and evaluation of 8 additional DFG-out allosteric inhibitors that were developed directly from fragments of these successful scaffolds.

Published by Elsevier Ltd.

1. Background

Gleevec®, which was developed as an inhibitor of c-Abl and the constitutively active fusion protein form Bcr/Abl,[1–3] was approved for the treatment of chronic myeloid leukemia (CML) in 2002. Gleevec® was the first compound shown to inhibit a kinase by binding the DFG-out allosteric site.[4] This site is actually just an inactive conformation of the enzyme characterized by movement of an AspPheGly (DFG) loop.[5] This movement is common to all DFG-out inhibitors and is depicted from structures of p38α in Figure 1. The position of the phenyl ring of phenylalanine determines whether the kinase is in the active or inactive conformation. In the active conformation (DFG-in), which the phosphorylated protein frequents approximately 80% of the time, the phenyl ring is contained in a hydrophobic pocket[6,7] (Fig. 1A). In this conformation, the triphosphate of ATP binds by utilizing two magnesium cofactors and aspartate from the DFG loop. In the inactive conformation (DFG-out), however, rearrangement of the DFG loop allows the phenyl ring to void the hydrophobic pocket as it rotates around the C–N bond of aspartate, displacing itself >10 Angstroms and into the ATP binding pocket (Fig. 1B). Because the phenyl ring of phenylalanine occupies the space usually utilized to bind ATP, the DFG-out conformation is mutually exclusive with ATP binding and thus renders the kinase in an inactive state.

DFG-out inhibitors stabilize the DFG-out conformation by placing a lipophilic group into the voided hydrophobic pocket, resulting in an increase in the population of inactive kinase. DFG-out allosteric inhibitors typically bridge from this site into the hinge region, the area normally occupied by ATP. Because allosteric site inhibitors bind an inactive conformation of the enzyme and do not compete directly with ATP or substrate, they can offer a significant kinetic advantage over ATP competitive inhibitors.[7]

Nexavar® (sorafenib, BAY 43-9006) is a potent inhibitor of B-Raf, which is currently approved for the treatment of renal cell carcinoma and is still undergoing multiple clinical trials in thyroid and liver cancers.[8–13] B-Raf kinase is mutated in approximately 7% of all human cancers with higher occurrence in 66% of human melanomas, 45% of sporadic papillary thyroid cancers, 33% of KRAS mutated pancreatic cancers, and 15% of sporadic colorectal cancers.[14–19] In a manner similar to Gleevec®, this agent inhibits by binding the inactive conformation of B-Raf characterized by a DFG loop move. Interestingly, Nexavar®, like Gleevec®, is not a specific inhibitor of its primary target enzyme, but also displays good inhibitory activity for the kinase domain of the vascular endothe-

* Corresponding author. Tel.: +1 520 626 5622; fax: +1 520 626 4824.
E-mail addresses: dietrich@pharmacy.arizona.edu (J. Dietrich), hurley@pharmacy.arizona.edu (L.H. Hurley).

0968-0896/$ - see front matter Published by Elsevier Ltd.
doi:10.1016/j.bmc.2010.05.063

lial growth factor receptor (VEGFR) and platelet derived growth factor receptor beta (PDGFRB), which allows this inhibitor to also promote anti-angiogenic effects much like the effects seen in the antagonism of the VEGF receptor by Avastin®.[20] The promising clinical efficacy of Nexavar® is attributed to the combination of inhibiting VEGFR1-2, PDGFR-β, and B-raf.[21,22]

BIRB-796 is a highly potent inhibitor of p38α,[23] a serine/threonine mitogen activated protein kinase (MAPK) that is usually associated with inflammation because of its role in T-cell proliferation and cytokine production.[24] The p38 pathway, however, factors into many other cellular events including proliferation, apoptosis, and cell differentiation.[21,22,25–28] BIRB-796, like Gleevec® and Nexavar®, binds a highly lipophilic selectivity site created by movement of the DFG loop. This inhibitor, developed as a treatment for rheumatoid arthritis and Crohn's disease, was withdrawn from phase III clinical trials.[29] Efforts in the pursuit of this inhibitor, however, yielded some very pertinent structural data that parallels other type 2 inhibitors. Kinetic data generated during the discovery of BIRB-796 established the slow binding kinetics of DFG-out inhibitors[7] and also highlighted that some allosteric inhibitors can display the ability to induce a conformation in which both the activated enzyme can be potently inhibited and the unphosphorylated enzyme can not be activated by phosphorylation on the activation loop.[30]

2. Structural requirements for allosteric inhibitors

The three DFG-out allosteric kinase inhibitors described share a basic architecture for construction that can be defined by four key interactions (Fig. 2).

2.1. Hydrogen-bonding interactions with the core scaffold

A critical inhibitor interacting group is the core or scaffold, which establishes a bridging hydrogen-bond network between a conserved glutamate side chain and the amide N–H from the aspartate involved in the DFG loop move (Fig. 2). In Gleevec®, this core scaffold is a benzamide (Fig. 2a), in Nexavar® a phenyl urea (Fig. 2b), and in BIRB 796 it is a pyrazole urea (Fig. 2c). The carbonyl from the urea or amide accepts a hydrogen-bond from the backbone NH of aspartate and the NH from the urea or amide forms a hydrogen-bond to the side chain of the conserved glutamate.

2.2. Hydrophobic interactions in the allosteric binding region

Hydrophobic interactions are made in the allosteric binding region within two selectivity sites. In the depicted binding orientation, the lower selectivity site is created when the phenyl alanine of the DFG loop flips out of its lipophilic pocket during the DFG loop move. The lower selectivity site is highly conserved among kinases that are approachable through allosteric inhibition. The upper selectivity site is less conserved and offers a unique position to build in selectivity. The core scaffold usually binds between the two selectivity sites and projects lipophilic moieties into the large hydrophobic pockets. When Gleevec® binds to Abl, a phenyl ring occupies space in the lower selectivity pocket and projects a *N*-methyl piperazine into the outer rim of the allosteric binding region (Fig. 2a). Nexavar® has a phenyl ring which is substituted with a trifluoromethyl group at the meta position that projects into the lower selectivity site (Fig. 2b). A *para*-chloro substituent also adds hydrophobicity to the phenyl ring and positively interacts with lower hydrophobic selectivity site when Nexavar® binds. BIRB-796 has a pyrazole scaffold that places a lipophilic *t*-butyl group into the lower selectivity site and a tolyl ring into the upper selectivity site (Fig. 2c). Of the three molecules, BIRB-796 is the only one to utilize the upper selectivity site.

2.3. Hydrophobic interactions in the gatekeeper region

The third interaction site is called the 'gatekeeper region' which is close to a conserved lysine side chain that is normally involved in triphosphate binding with ATP. As a result of the DFG loop movement, the phenylalanine side chain of this loop typically closes off the gatekeeper region forming a distinct hydrophobic binding site. An aromatic ring spans this region in all three inhibitors. Gleevec® (Fig. 2a) and Nexavar® (Fig. 2b) utilize a phenyl ring and BIRB-796 utilizes a larger naphthyl ring to bind the gatekeeper region (Fig. 2c).

2.4. Hydrogen-bonding interactions with the hinge region

All three inhibitors bind to the hinge region where the adenine ring of ATP normally binds and accepts a hydrogen-bond from the hinge region. In Gleevec® a 3-pyridyl ring is used (Fig. 2a), in Nexavar® a *N*-methyl-4-picolinamide (Fig. 2b), and in BIRB-796 a morpholino group (Fig. 2c).

When evaluating the crystal structure of these three inhibitors bound to their target enzyme, it is not obvious where selectivity can be achieved because there are many similar binding interactions. This point is exasperated in a recent report by Namboodiri et al. in which the authors report crystal structures in which Gleevec® and Nexavar® are bound to p38α.[31] In this study, we report the enzymatic selectivity of Gleevec®, Nexavar®, and BIRB-796® with respect to c-Abl, B-Raf, and p38α. Although the selectivity

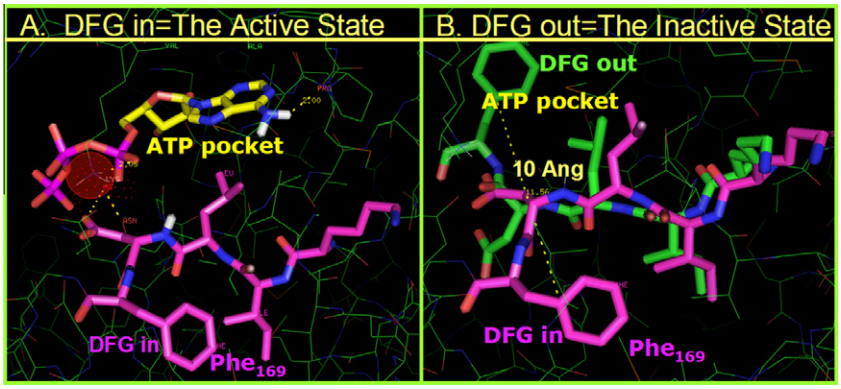

Figure 1. Conformation DFG-in and DFG-out. (A) The DFG-in active state (magenta) of p38α with ATP bound in the ATP pocket. The three phosphates and the side chain of aspartate complex to the Mg^{2+} cofactor. (B) The phenyl ring of Phe_{169} in the active state (magenta) rotates around the CN bond of Asp_{168} and positions the phenyl ring 10 Å away and into the ATP pocket. This movement results in the DFG-out inactive state shown in green.

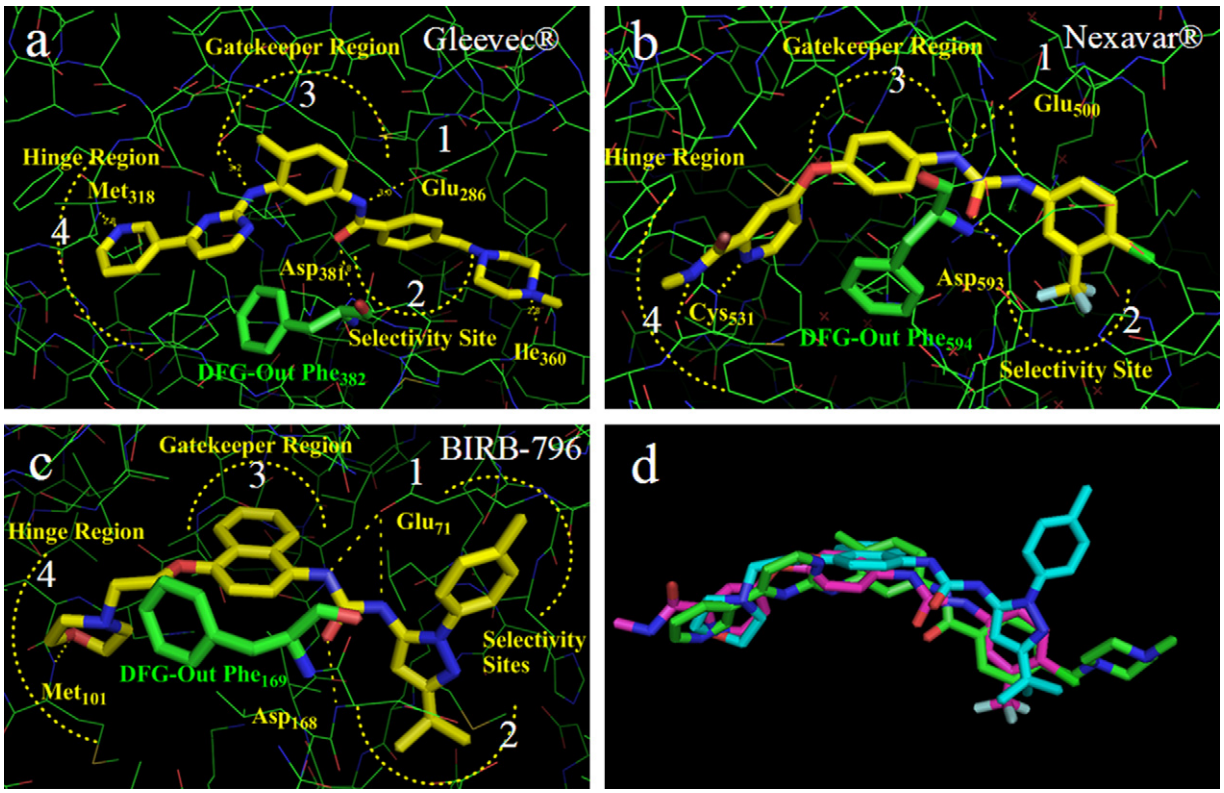

Figure 2. Crystal structures of known allosteric kinase inhibitors. (a) Crystal structure of Gleevec® (imatinib, STI571) bound Abl kinase (PDB: 1IEP). (b) Crystal structure of Sorafenib (Nexavar®, BAY 43-9006) bound to B-Raf kinase (PDB: 1UWJ). (c) BIRB-796 bound to p38α kinase (PDB: 1KV2. (d) Overlap of Gleevec® (green), sorafenib (mauve), and BIRB-796 (teal) in their bound conformations. (1) Hydrogen-bonding interactions with the core scaffold. (2) Hydrophobic interactions in the allosteric binding region. (3) Hydrophobic interactions in the gatekeeper region. (4) Hydrogen-bonding interactions with the hinge region.

of these inhibitors has been previously published,[32–34] To further our study and gain additional information, we have broken these three molecules down into three distinct fragments (Fig. 3). One fragment consists of the left side of the central core which binds to the gatekeeper and hinge regions. The second fragment is the central core, and the third fragment is the right side of the central core that binds to the selectivity sites in the allosteric binding region. In order to distinguish which fragment of each molecule contributes to selectivity among the three kinases of interest, we synthesized 8 hybrid molecules (Fig. 4) that combine the different fragments of each known inhibitor and evaluated their inhibitory activity with respect to c-Abl, B-Raf, and p38α.

Previously described methods were used to synthesize Nexavar®,[35] BIRB-796,[7] and Gleevec®.[36] Major intermediates from the three previous synthetic routes were utilized in the synthesis of 6 of the 8 hybrid molecules (Scheme 1). Important gatekeeper and hinge region binding amine intermediates include compound **12**, **13**, and **14** (Scheme 1). The right sides of hybrid molecules were derived from isocyanate **16** from sorafenib, 5-*tert*-butyl-2-p-tolyl-2H-pyrazol-3-yl-amine (**17**) from BIRB-796, and 4-[(4-methylpiperazin-1-yl)methyl]benzoyl chloride dihydrochloride (**18**) from Gleevec®. Urea and amide linkages were made using the standard coupling methods as were previously described in the syntheses of Nexavar, BIRB-796, and Gleevec®.

The synthesis of **10** (Scheme 2) is described in Scheme 2. The amination of 1-bromomethyl-4-nitrobenzene (**18**) by 4-*N*-methylpiperazine was accomplished in the presence of potassium carbonate in refluxing acetonitrile to yield 1-methyl-4-(4-nitrobenzyl)piperazine (**20**). The nitro group of **20** was then cautiously reduced via hydrogenation under 30 psi hydrogen gas in the presence of 10% palladium on carbon in ethanol to give the corresponding amine (**21**). The urea linkage was assembled by the reaction of

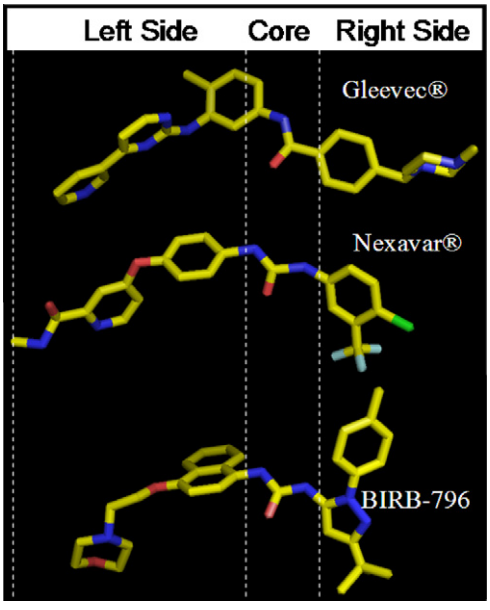

Figure 3. Breakdown of allosteric kinase inhibitors.

21 with the preformed *N*-imidazole carboxamide **22** in dichloromethane at room temperature to yield the target molecule **10**.

The synthesis of compound **11** was accomplished through the route described in Scheme 3. The potassium-4-nitro-phenoxide (**24**) was generated from reaction of nitrophenol in ethanol in the presence of potassium hydroxide. After isolation of **24**, the ether linkage was incorporated in the molecule by reaction with

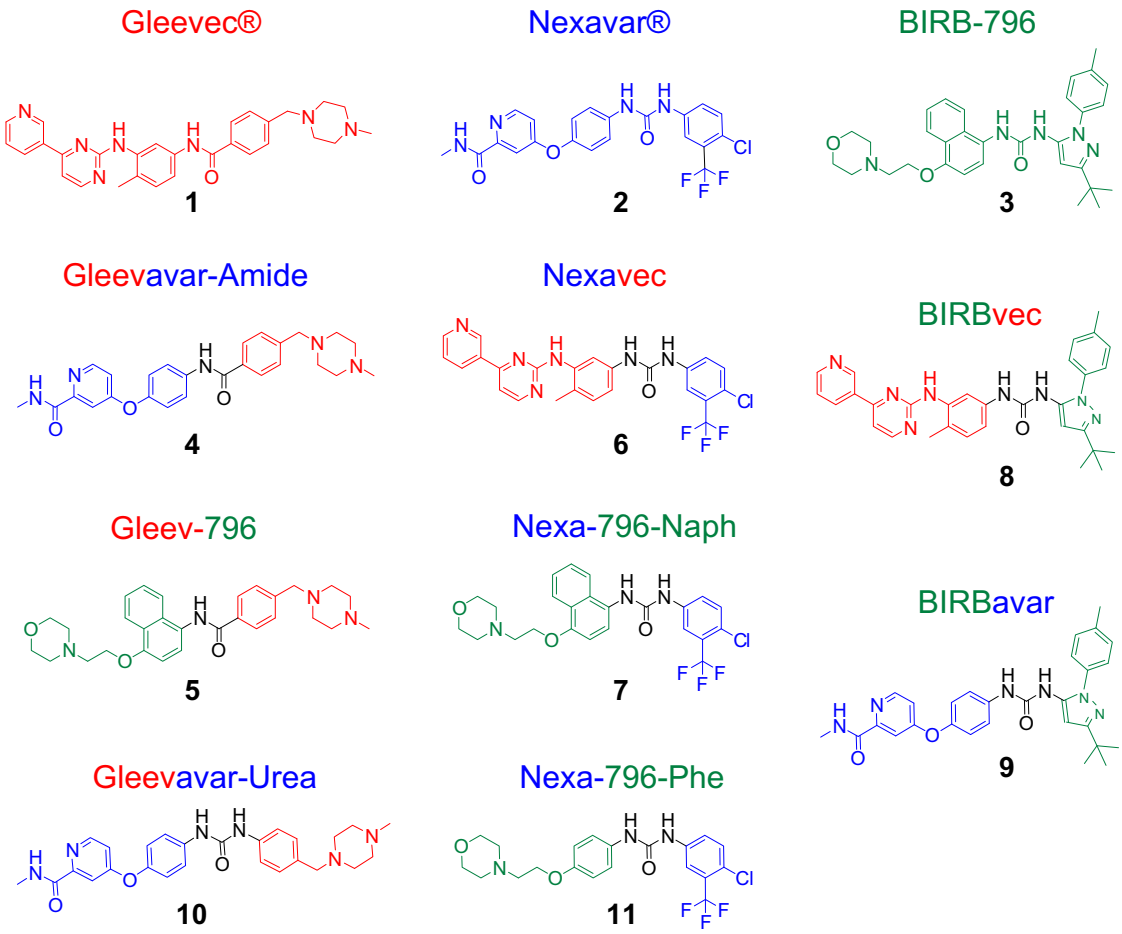

Figure 4. Parent and hybrid molecules that were synthesized and evaluated. Gleevec® is shown in red, Nexavar in blue, and BIRB-796 in green. The hybrid molecules are depicted as a combination of colors to represent which part came from which parent molecule. The naming scheme names the right side of the molecule first and the left side second, that is, Gleev-796 (**5**) has the right side of Gleevec® and the left side of BIRB-796.

4-(2-chloroethyl)morpholine in refluxing toluene to afford 4-(2-(4-nitrophenoxy)ethyl)morpholine (**25**) in modest yield.[37] The nitro group was then reduced via hydrogenation with 10% palladium on carbon to yield amine **26**. The urea linkage was then accomplished by reaction of 26 with isocyanate **16** in dichloromethane.

3. Results and discussion

All of the molecules that were synthesized for this study were evaluated in three radiometric kinase assays: one for p38α, one for B-Raf, and one for Abl kinase. The p38α and B-Raf assays utilized human recombinant GST-tagged enzymes purchased from invitrogen, 100 μM ATP, and full length recombinant inactive substrate kinase since these kinases have the ability to form ternary structures with their substrate kinase. The Abl kinase assays utilized mouse GST-tagged c-Abl, the peptide substrate Abltide, and 100 μM ATP.

The initial enzymatic inhibition results from Gleevec®, Nexavar®, and BIRB-796 (Table 1, compounds **1–3**) showed that among the three allosteric kinase inhibitors, Gleevec® was the most specific for its target enzyme c-Abl, exhibiting an IC_{50} of 10.8 nM and showing no inhibitory activity against either p38α or B-Raf at a 100 μM concentration. BIRB-796 showed the most potency for its target enzyme p38α with an IC_{50} of 4.0 nM, but also inhibited B-Raf with an IC_{50} of 83 nM and Abl with an IC_{50} of 14.6 μM. Nexavar® was the least selective and showed strong inhibition in all three kinase assays, inhibiting its target enzyme B-Raf with an IC_{50} of 76.2 nM, p38α with an IC_{50} of 84.8 nM, and Abl with an IC_{50} of 225.9 nM.

Although the data in Table 1 clearly shows that these three inhibitors have very different selectivity profiles, there is not enough data and too many variables to ascertain what moieties in the molecules are responsible for the selectivity profile of each inhibitor. The enzymatic inhibition profiles of the hybrid molecules, however, can more clearly decipher where the selectivity is coming from. It is possible to ascertain which portion of the molecule is responsible for the selectivity by making modifications to each region of the molecule and evaluating which modification results in a loss of selectivity.

Since Gleevec® is the most selective of the three compounds, hybrid molecules that contain a moiety from Gleevec® were evaluated first (Table 1, molecules with red). When Gleevec® (**1**) or hybrid molecules such as compounds **4**, **5**, and **10** utilized the 1-benzyl-4-methylpiperazine from the right side of Gleevec®, they could not inhibit the enzymatic activity of p38α or B-Raf at a 100 μM concentration—even when the 4-(2-morpholinoethoxy)naphthyl group from the potent p38α inhibitor BIRB-796 was incorporated (**5**) or the *N*-methyl-phenoxypicolinamide group from Nexavar® was used (**4**).

On the other hand, when the left side of Gleevec® was used, as seen in compounds **6** and **8**, then the molecules were able to inhibit p38α and B-Raf. Compound **6** has a urea linkage and the *meta*-trifluoromethyl-*para*-chlorophenyl ring from Nexavar® and inhibits 50% of the activity of c-Abl at less than 1 nM, p38α at 18.4 nM,

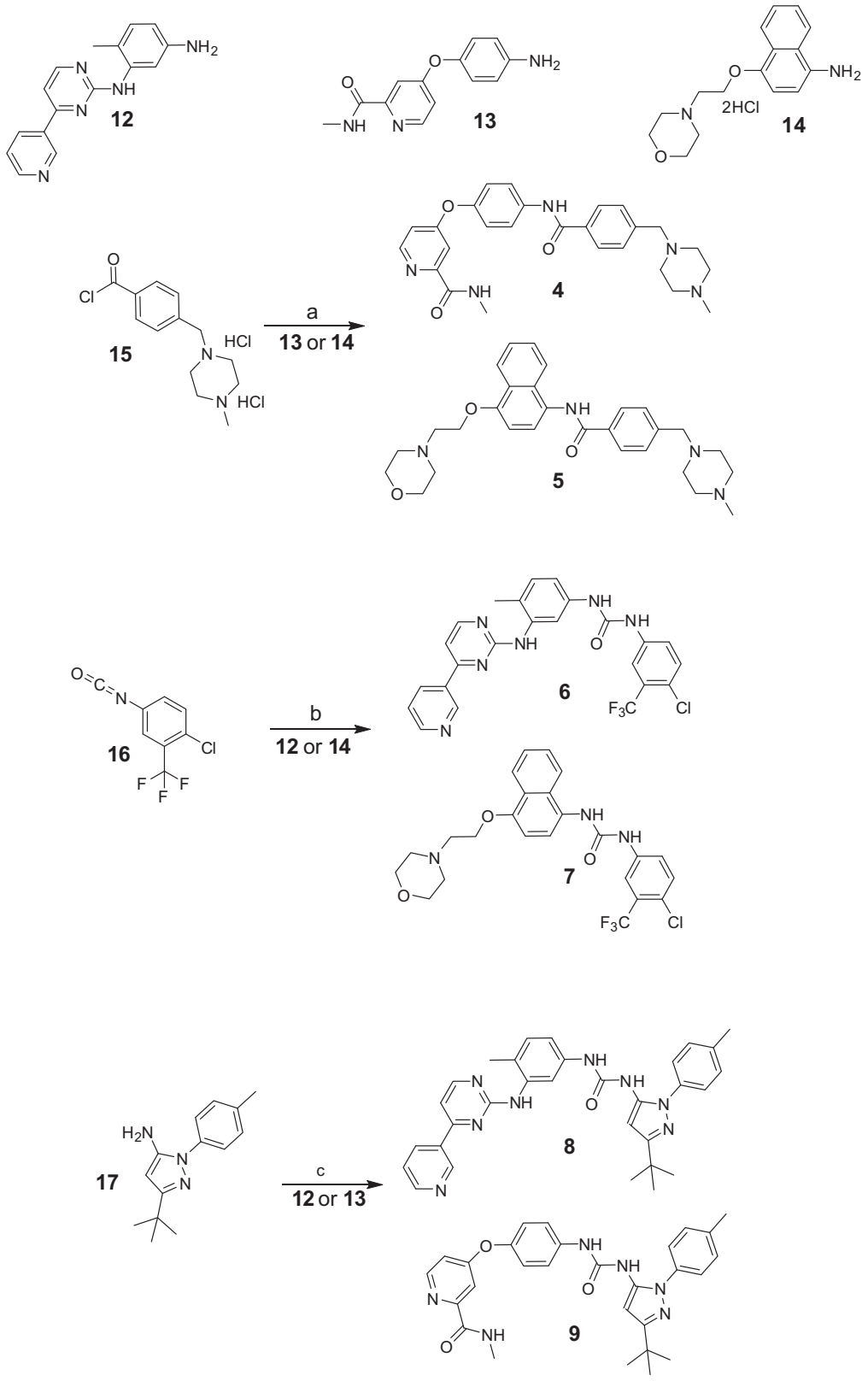

Scheme 1. Synthesis of hybrid molecules. Reagents and conditions: (a) **13** or **14**, pyridine, 50 °C, 12 h; (b) **12** or **14**, DCM, TEA, 12 h; (c) phosgene, 4 h, then **12** or **13**, 12 h.

and B-Raf at 180 nM. Compound **8** has a urea linkage and the 5-*tert*-butyl-2-*p*-tolyl-2*H*-pyrazol-3-yl ring from BIRB-796 and inhibits c-Abl with an IC_{50} of 8.6 nM, p38α with an IC_{50} of 183.9 nM, and B-Raf with an IC_{50} of 413.9 nM. From this data, it is apparent that the selectivity of Gleevec® to only inhibit c-Abl and not B-Raf or p38α comes from the 1-benzyl-4-methylpiperazine moiety that binds in the allosteric binding region of c-Abl. This observation has previously been reported by Baldwin et al. in which compounds containing a *N*-methyl-piperazine did not show any inhibition of p38α activity.[38]

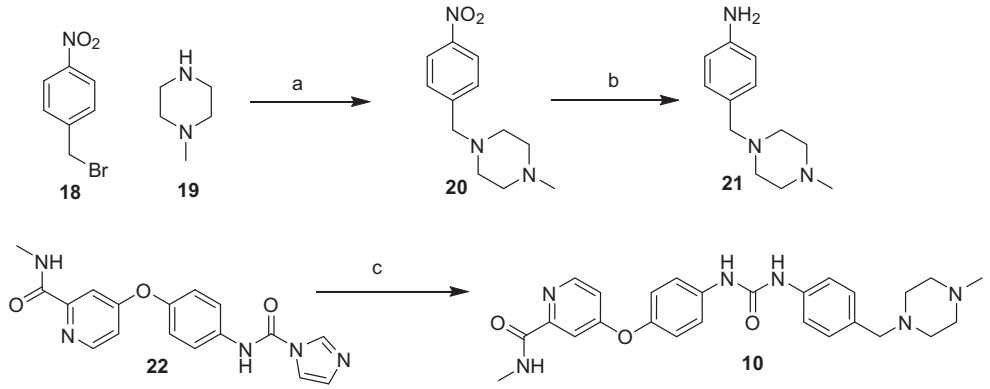

Scheme 2. Synthesis of compound **10**. Reagents and conditions: (a) K_2CO_3, MeCN, reflux, 18 h, 45%; (b) 30 psi H_2 gas, 10% Pd/c, EtOH, 2 h, 99%; (c) **21**, DCM, rt, 24 h, 78%.

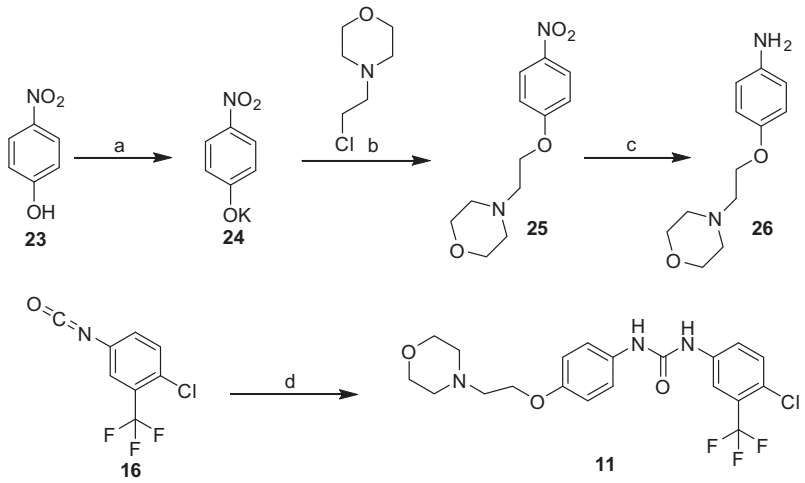

Scheme 3. Synthesis of compound **11**. Reagents and conditions: (a) KOH, EtOH, rt, 2 h, 90%; (b) 4-(2-chloroethyl)-morpholine, toluene, reflux, 24 h, 54%; (c) 50 psi H_2, 10% Pd/c, EtOH, 1 h, 99%; (d) DCM, rt, 18 h, 65%.

If this hypothesis is true, it is expected to find a structural difference in the crystal structures of c-Abl, p38, and B-Raf that can explain the molecular reason for this selectivity. In Gleevec®, the methyl piperazine sits deeply into the selectivity site and in its biologically prevalent protonated form makes two hydrogen-bonds with the backbone carbonyls of isoleucine 360 and histidine 361 (Fig. 5). Two methylene carbons in the piperazine ring make van der Waals interactions with the side chain benzyl methylene of phenylalanine 359. As depicted by the overlay of B-Raf with c-Abl (Fig. 5), the selectivity site residues are highly homologous. In B-Raf and p38α, the analogous position to phenylalanine 359 in c-Abl is instead an isoleucine (p38α ILE146, B-Raf ILE571), which directs the isolated methyl group into the analogous space piperazine occupies in c-Abl and blocks the binding pocket. This finding is further supported by the resistance profiles of patients that are prescribed Gleevec®. A rare but very serious single nucleotide substitution at codon 359 that replaces phenylalanine with an isoleucine can occur in patients that receive Gleevec® therapy and this single mutation results in complete resistance to Gleevec® chemotherapy.[39] The same residue that is responsible for the selectivity of Gleevec® over p38 and B-Raf is an Achilles' heel, that if mutated, will also knock out inhibition of c-Abl.

The same type of analysis can be performed with BIRB-796 if the right side of BIRB-796 is held constant with the 5-*tert*-butyl-2-*p*-tolyl-2*H*-pyrazol-3-yl group from BIRB-796 (Table 1, compounds **3**, **8** and **9**) and the left side is modified. Compounds **8** and **9** display potent inhibitory activity for c-Abl with IC_{50}'s of 8.6 nM and 62.6 nM. The inhibitory activity of these molecules is much lower for B-Raf. Compound **8** inhibits B-Raf with an IC_{50} of 413.9 nM and compound **9** inhibits B-Raf with an IC_{50} of 236.7 nM. These results suggest that the large 5-*tert*-butyl-2-*p*-tolyl-2*H*-pyrazol-3-yl moiety from BIRB-796 binds unfavorably to the allosteric binding region of B-Raf and a large hydrophobic moiety engineered into molecules to bind this region can be used to make a p38α inhibitor selective over B-Raf because the overall size of the hydrophobic selectivity sites in B-Raf is smaller.

When the left side of molecules utilized the 4-(2-morpholinoethoxy)naphthyl group from BIRB-796 (Table 1, compounds **3**, **5**, and **7**) and the right sides of the molecules were changed, it was apparent that the 4-(2-morpholinoethoxy)naphthyl group does not bind favorably with c-Abl. In compounds **3**, **5**, and **7** (Table 1), the IC_{50}'s for c-Abl are all in the micromolar range. When comparing the p38 and B-Raf enzymatic inhibition data, the 4-(2-morpholinoethoxy)naphthyl group can make favorable interactions in both p38 and B-Raf. Compound **7** is a very potent inhibitor of both p38 and B-Raf with IC_{50}'s for each enzyme below 1 nM.

To structurally evaluate the differences in the three kinases at the gatekeeper region, we superimposed the three crystal structures on top of each other and evaluated this portion of the molecule and found that the naphthyl ring from BIRB-796 pushes very deep into the gate keeper region. At the deepest part of this region in p38α, leucine 104 makes hydrophobic interactions with the naphthyl ring (Fig. 6). In c-Abl, however, this position is instead isoleucine 313 which decreases the size of the hydrophobic pocket by

Table 1
Complete enzymatic results (results were calculated from the average of $n \geqslant 2$ independent experiments performed in duplicate with R^2 >0.93)

		M.W.	*c*Log *P*	IC50 Abl nM	IC50 B-Raf nM	IC50 p38a nM
Gleevec® **1**	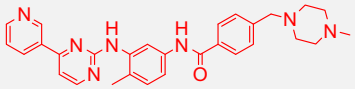	493	3.83	10.8	>100,000	>100,000
Nexavar® **2**	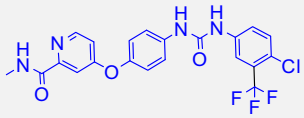	464	3.76	225.9	76.2	84.8
BIRB-796 **3**	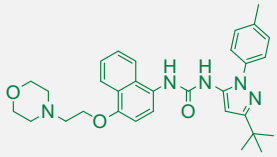	527	5.79	14600.0	83.4	4.0
GleevAvar **4**	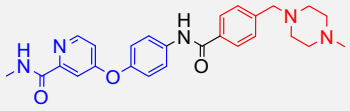	459	2.30	>30,000	>100,000	>100,000
Gleev-796 **5**	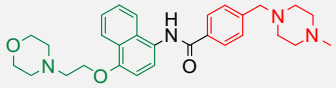	488	3.01	>30,000	>100,000	>100,000
NexaVec **6**	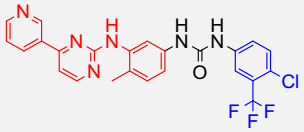	498	5.28	<1	180.1	18.4
Nexa-796 **7**	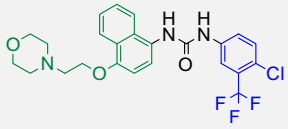	493	4.46	12930.0	<1	<1
BIRBvec **8**	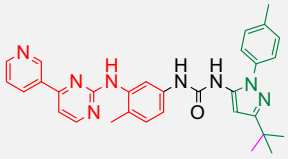	532	6.61	8.6	413.9	189.3
BIRBavar **9**	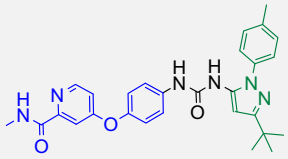	498	5.08	62.6	236.7	<1
Gleevavar-Urea **10**	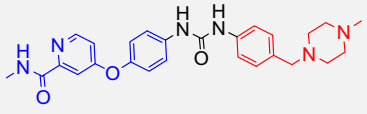	474	3.61	572.4	>100,000	>100,000
Nexa-796-Phe **11**	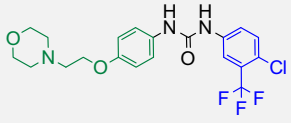	443	5.10	244.0	92.3	105.5

projecting the isolated methyl group into the hydrophobic pocket. Consequentially, the gatekeeper region of c-Abl is responsible for the unfavorable binding of BIRB-796 to c-Abl.

To further investigate this hypothesis, compound **11** (Table 1) was synthesized, which contained a morpholinoethoxy phenyl group instead of the morpholinoethoxy naphthyl group. Compound **11** is identical to compound **7** except for the naphthyl ring in compound **7** is changed to a smaller phenyl ring. Compound **11** was able to rescue c-Abl activity (IC_{50} = 244.0 nM) and provided evidence that the naphthyl ring was too large to fit into the gatekeeper region of c-Abl. Compound **7** (Table 1) displayed subnanomolar potency for both p38α and B-Raf and has a naphthyl ring in the gatekeeper region, however, when the smaller phenyl ring was used in compound **11**, the potency decreased (IC_{50BRaf} = 92.3 nM, IC_{50p38} = 105.5 nM) indicating that there are favorable hydrophobic binding interactions when a naphthyl ring is utilized to bind to the gatekeeper region of B-Raf and p38α.

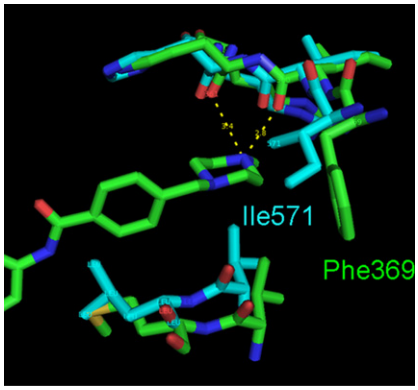

Figure 5. Overlap of c-Abl (1IEP) with B-Raf kinase (PDB: 1UWJ). c-Abl and Gleevec are shown in green. B-Raf kinase is shown in teal. Isoleucine 571 is not compatible with Gleevec® binding to B-Raf. A single residue difference at this position is responsible for the ability of Gleevec® to select c-Abl over p38α and B-Raf kinase.

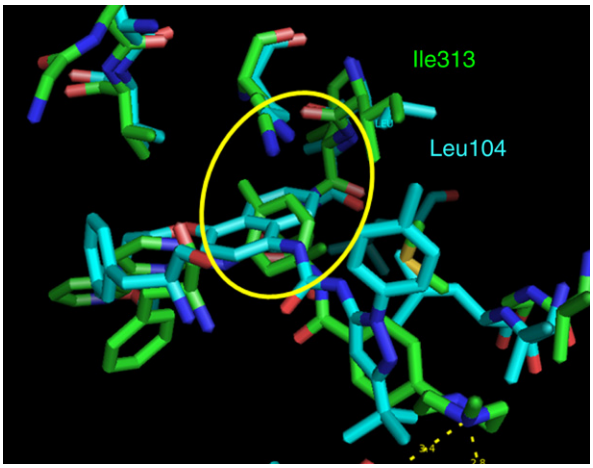

Figure 6. Overlap in the gatekeeper region of cAbl and p38α. Gleevec® and c-Abl (PDB: 1IEP) is shown in green and BIRB-796 and p38 (PDB: 1KV2) is shown in teal.

Nexavar® is the least selective inhibitor of the three. When the *meta*-trifluoromethyl-*para*-chlorophenyl ring is utilized to make inhibitors (compounds **2**, **6**, **7**, **11**) and the left side is modified, it is possible to make subnanomolar inhibitors for all three kinases (Table 1). Compound **6** is a subnanomolar inhibitor of c-Abl and compound **7** is a subnanomolar inhibitor of both p38α and B-Raf. Because this moiety can be used to make potent inhibitors for all three target kinases, it is prudent to conclude that this moiety binds well to the allosteric binding region of all three kinases. As discussed previously, the data collected for compounds **3**, **8**, and **9** indicates that B-Raf has a smaller allosteric binding region than p38 and c-Abl. As a result of this, a B-Raf inhibitor must have a smaller moiety in this region and consequentially cannot select B-Raf kinase over p38 or c-Abl.

When the left side of hybrid molecules utilized the *N*-methyl-4-phenoxy-picolinamide moiety from Nexavar® (compounds **2**, **4**, **9**, **10**) and the right side is modified, it is possible to make potent inhibitors for all three targets as well. Nexavar® itself is a potent inhibitor of both B-Raf (IC_{50} = 76.2 nM) and p38 (IC_{50} = 84.8 nM) and a slightly less potent inhibitor of c-Abl (IC_{50} = 225.9). Compound **9**, which also utilizes the *N*-methyl-4-phenoxy-picolinamide is also a potent inhibitor of all three kinases. The broad spectrum inhibition of Nexavar® can be attributed to the ability of both the right side and left side of Nexavar® to bind with high affinity to all three kinases.

It was surprising that compound **4** did not show any inhibition of c-Abl at 30 μM. We hypothesized that this was due to having an amide in the core instead of a urea. Compound **10**, which is identical to compound **4** except for that it has a urea in the core instead of an amide, was synthesized to explore this hypothesis. When this compound was tested, it expectedly showed no inhibition of p38α and B-Raf at 100 μM, but modestly inhibited c-Abl with an IC_{50} of 572.4 nM. When the urea scaffold is used with the *N*-methyl-4-phenoxypicolinamide moiety on the left, it can make favorable binding interactions in the hinge region, but as a consequence of the longer linkage, the interactions in the allosteric binding region by the 1-benzyl-4-methylpiperazine from Gleevec® are then aberrantly modified. As discussed earlier and depicted in Figure 5, the *N*-methylpiperazine ring sits in a very tight pocket and any modification at this region can result in a steric interaction that is not favorable for binding.

4. Summary and conclusions

The research presented here evaluates the structural overlap of three DFG-out allosteric kinase inhibitors, Gleevec®, Nexavar®, and BIRB-796, bound to their primary target, C-Abl, B-Raf, and p38α. These known molecules were broken down into three distinct regions and 8 hybrid molecules were synthesized that were derived directly from the scaffolds of these successful inhibitors (Figs. 3 and 4). Enzymatic inhibition results from the known inhibitors and the 8 hybrid DFG-out inhibitors gave insight into the regions of these molecules and kinases that promote selectivity or broad range inhibition (Fig. 7).

In the selectivity site, which is available upon the DFG rearrangement, the 3-trifluoromethyl-4-chlorophenyl ring found in Nexavar® can make favorable interactions in all three kinases. When this moiety is changed to a larger moiety such as the 5-*tert*-butyl-2-*p*-tolyl-2*H*-pyrazole as found in BIRB-796, this tends to alleviate B-Raf binding and favors binding to p38α and Gleevec®.

When Gleevec® binds to C-Abl, the selectivity site is occupied by a 1-benzyl-4-methylpiperazine. In this system, the *N*-methylpiperazine ring binds to the outer edge of the selectivity sites and donates two hydrogen-bonds to carbonyls from the backbone of the protein. The carbons of the piperazine ring make a positive and unique van der Waal's interaction with Phe369. In p38α and B-Raf, this interaction is not possible because the analogous position contains an isoleucine that blocks the pocket in which the *N*-methylpiperazine ring of Gleevec® binds c-Abl.

Placing a large naphthyl ring in the gatekeeper region makes favorable interactions with p38α and B-Raf, however, Abl contains a smaller hydrophobic pocket. The naphthyl ring in BIRB-796 is responsible for the selectivity of p38α over c-Abl.

Aside from the structural data that was gathered from synthesizing and evaluating these molecules, we have also created 8 new chemical entities that have varying attributes such as novel selectivity profiles, increased potency, and/or favorable drug-like properties. Compounds **6**, **8**, and **9** are all potent inhibitors of c-Abl and structurally represent novel compounds that could predictably inhibit mutated forms of BCR-Abl that are resistant to Gleevec® inhibition. These studies are ongoing and will be reported separately in due course. Compound **7** (Table 1) is a novel, subnanomolar inhibitor of p38 and B-Raf kinase and could be explored for its utility in targeting B-Raf mutated cancers.

This research highlights that selectivity in kinase inhibitors is a reachable goal if inhibitors are engineered to exploit minor differences among kinases. A very simple one residue difference in the allosteric binding region of c-Abl allows Gleevec® to be selective for c-Abl over p38α and B-Raf. Another one residue difference in the gatekeeper region of p38 allows BIRB-796 to be selective for p38α over c-Abl. Finding unique differences among kinases and

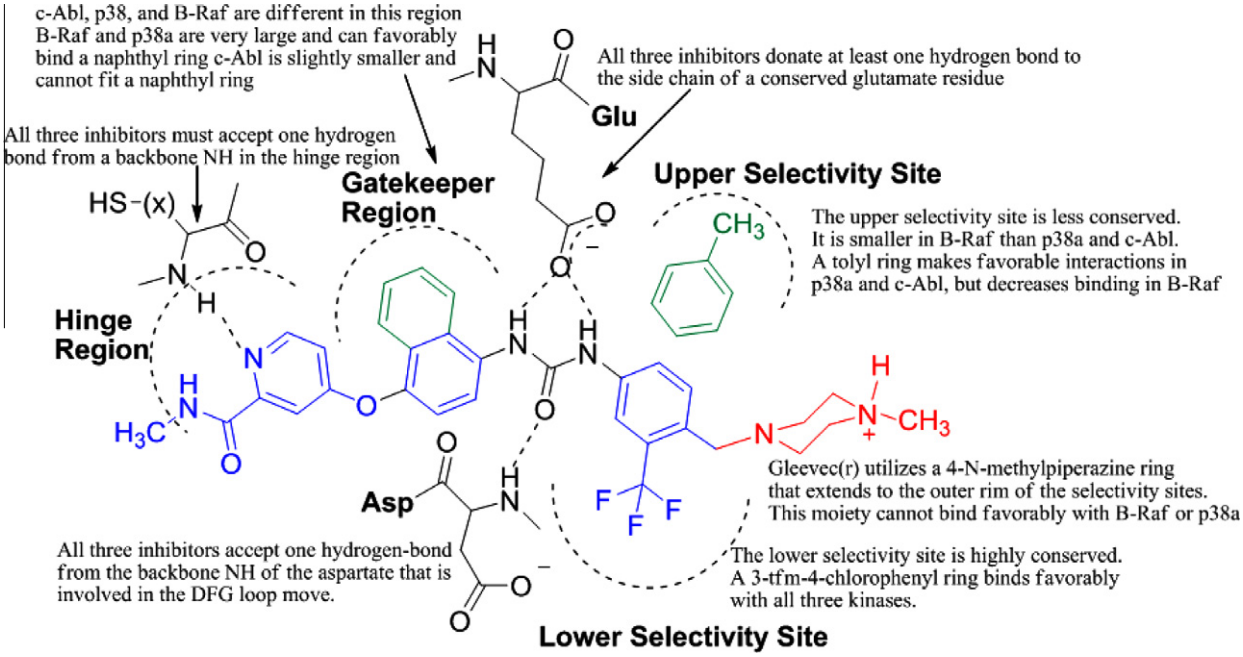

Figure 7. Schematic of specific binding interactions in Gleevec®, Nexavar®, and BIRB-796. Red represents atoms from Gleevec®, blue represents atoms from Nexavar®, and green represents atoms from BIRB-796.

kinase inhibitors that render selectivity is only the first battle. As it becomes more possible to design molecules with a desired kinase profile, the next stage will have to address which profile is the most desirable.

5. Experimental procedures

5.1. Chemistry

^{1}H NMR and ^{13}C NMR spectra were recorded on Bruker Avance spectrometer at 300 and 75 MHz, respectively, with TMS as an internal standard. HRMS experiments were performed on a Q-TOF-2TM (Micromass). TLC was performed with Merck 60 F254 silica gel plates. Column chromatography was performed using a Biotage SP1 system with manually loaded 12-, 25-, or 40-g columns. The purity of the target compounds was determined to be >95% by LC/MS on a Series 1100 LC/MSD (Agilent Technologies, Palo Alto, CA) equipped with a vacuum de-gasser (G1322A), a binary pump (1312A), an autosampler (G1313A), a thermostated column compartment (G1316A), and a mass selective detector (G1946A) supplied with atmospheric pressure ionization electrospray (API-ES). LC/MS utilized a Zorbax® C18 SB column (3.5 μm, 4.6 × 150 mm), MeCN/HOH/HAc (pH 4.8) elution buffer, and 15-min runs. Mass spectra and high resolution mass spectra were obtained using an ESI method by the Mass Spectroscopy Facility in the Chemistry Department at the University of Arizona. All solvents and reagents were purchased from Aldrich, TCI America, Matrix Scientific, and Ryan Scientific and used without further purification or drying.

5.2. Preparation of hybrid molecules

5.2.1. *N*-Methyl-4-(4-(4-((4-methylpiperazin-1-yl)methyl)-benzamido)phenoxy)picolinamide (Gleevavar-Amide, 4)

117 mg 4-((4-methylpiperazin-1-yl)methyl)benzoyl chloride dihydrochloride (0.357 mmol, 1 equiv) and 100 mg **15** (0.357 mmol, 1 equiv) was reacted in 5 mL pyridine for 14 h and then poured onto 50 g ice. The mixture was allowed to cool and a precipitate formed that was collected by vacuum filtration and purified by flash chromatography through a silica gel column on a Biotage Sp1 system (3–8% MeOH/DCM) to yield 106 mg **4** (0.231 mmol, 64.5% yield). ^{1}H NMR (300 MHz, DMSO-d_6): δ 10.57 (s, 1H), 8.83 (q, 1H, J = 4.8 Hz), 8.52 (d, 1H, J = 5.5 Hz), 8.05 (d, 2H, J = 8.2 Hz), 7.95 (d, 2H, J = 9.0 Hz), 7.82 (d, 2H, J = 7.1 Hz), 7.41 (d, 1H, J = 2.5 Hz), 7.26 (d, 2H, J = 8.5 Hz), 7.19 (q, 1H, J = 1.5 Hz), 4.44 (s, 2H), 3.61 (br, 8H), 2.81 (s, 3H), 2.78 (d, 3H, J = 4.6 Hz). ^{13}C NMR (75 MHz, DMSO-d_6): δ 166.86, 165.83, 164.47, 153.08, 151.15, 149.66, 137.78, 136.33, 132.14, 128.96, 125.26, 123.11 (2c), 122.17 (2C), 115.02, 109.64, 65.87, 58.40 (2C), 51.29 (2C), 48.74, 26.90. HRMS (ESI) (M+1): 460.2343 calcd for $C_{26}H_{29}N_5O_3$ (M+1) = 460.2270.

5.2.2. 4-((4-Methylpiperazin-1-yl)methyl)-*N*-(4-(2-morpholino-ethoxy)-naphthalen-1-yl)benzamide (Gleev-796, 5)

141 mg 4-((4-methylpiperazin-1-yl)methyl)benzoyl chloride dihydrochloride (0.434 mmol, 1.5 equiv) and 100 mg **15** (0.290 mmol, 1 equiv) were reacted in 5 mL THF for 14 h and then poured into a separatory funnel that contained 50 mL sodium carbonate and 50 mL EtOAc. The organic layer was removed and the water layer was then extracted with another 50 mL of EtOAc. The combined organic layer was dried over $MgSO_4$ and concentrated to near dryness as a white solid. The product was very hygroscopic and was stored under nitrogen in a desiccator to prevent decomposition. ^{1}H NMR (300 MHz, DMSO-d_6): δ 10.17 (s, 1H), 8.19 (dd, 1H, J = 1.9 Hz, J = 7.7 Hz), 7.43–7.63 (m, 3H), 7.36 (d, 2H, J = 8.4 Hz), 7.97 (d, 2H, J = 8.4 Hz), 4.27 (t, 2H, J = 5.7 Hz), 3.41–3.60 (m, 6H), 2.88 (m, 2H), 2.2–2.6 (br d, 12 H), 2.23 (s, 3H), 2.06 (s, 3H). HRMS (ESI) (M+1): 489.2860 calcd for $C_{29}H_{36}N_4O_3$ (M+1) = 489.2787.

5.2.3. 1-(4-Chloro-3-(trifluoromethyl)phenyl)-3-(4-methyl-3-(4-(pyridin-3-yl)pyrimidin-2-ylamino)phenyl)urea (Nexavec, 6)

To a stirred solution of 100 mg (0.514 mmol, 1.25 equiv) 4-chloro-3-trifluoromethylaniline in 5 mL DCM was added 5 mL $NaHCO_3$ and the mixture was cooled to 0 °C in an ice bath. Stirring was stopped and 384 μL (0.617 mmol, 1.5 equiv) of a 20% solution of phosgene in toluene was added directly to the DCM layer via

syringe. Stirring was then continued for 4 h. 113 mg amine **12** (0.409 mmol, 1 equiv) was then added and the reaction was allowed to proceed for 14 h. The reaction was then dissolved in 50 mL EtOAc and subsequently washed with a saturated solution of sodium bicarbonate and then water. The crude material was dried onto silica, which was then loaded onto a silica gel column. The column was run on a Biotage Sp1 system (1–6%, MeOH, $CDCl_3$) to yield 158 mg **6** (0.317 mmol, 77% yield) as a light yellow solid.

^{1}H NMR (300 MHz, DMSO-d_6): δ 9.29 (d, 1H, 1.6 Hz), 9.10 (s, 1H), 8.90 (s, 1H), 8.77 (s, 1H), 8.69 (dd, 1H, J = 1.5 Hz, J = 4.7 Hz), 8.47–8.52 (m, 2H), 8.11 (d, 1H, J = 2.0 Hz), 7.83 (s, 1H), 7.58–7.65 (m, 2H), 7.51 (dd, 1H, J = 4.8 Hz, J = 7.9 Hz), 7.43 (d, 1H, J = 5.2 Hz), 7.15 (s, 1H), 2.21 (s, 3H). ^{13}C NMR (75 MHz, DMSO-d_6): δ 162.24, 161.86, 160.37, 153.26, 151.75, 148.61, 140.32, 138.78, 137.97, 135.85, 133.25, 132.81, 131.14, 127.51 (d, J = 30.7 Hz), 126.70, 124.84, 123.81, 123.67 (q, J = 273.3), 122.96, 117.49 (q, J = 5.9 Hz), 115.97, 115.75, 108.49, 18.38. HRMS (ESI) (M+1): 499.1295 calc. for $C_{24}H_{18}ClF_3N_6O$ (M+1) = 498.1183.

5.2.4. 1-(4-Chloro-3-(trifluoromethyl)phenyl)-3-(4-(2-morpholinoethoxy)-naphthalen-1-yl)urea (Nexa-796-Naph. 7)

To a stirred solution of 100 mg (0.514 mmol, 1.25 equiv) 4-chloro-3-trifluoromethylaniline in 5 mL DCM was added 5 mL $NaHCO_3$ and the mixture was cooled to 0 °C in an ice bath. Stirring was stopped and 384 μL (0.617 mmol, 1.5 equiv) of a 20% solution of phosgene in toluene was added directly to the DCM layer via syringe. Stirring was then continued for 4 h. 141 mg amine **14** (0.409 mmol, 1 equiv) was then added and the reaction was allowed to proceed for 14 h. The product precipitated from the reaction as a pink solid and was collected by suction filtration and subsequently washed with water and DCM. The light pink material was then dried in a vacuum oven at 60 °C for 6 h to yield 123 mg of **7** (60.9% yield). ^{1}H NMR (300 MHz, DMSO-d_6): δ 9.34 (s, 1H), 8.62 (s, 1H), 8.20 (dd, 1H, J = 1.3 Hz, J = 8.3 Hz), 8.14 (d, 1H, J = 2.5 Hz), 7.99 (d, 1H, J = 7.9 Hz), 4.28 (t, 2H, J = 5.7 Hz), 3.60 (m, 4H), 2.86 (t, 2H, J = 5.7 Hz), 2.56 (m, 4H). ^{13}C NMR (75 MHz, DMSO-d_6): ^{13}C NMR (75 MHz, DMSO-d_6): δ 154.40, 152.11, 140.59, 132.83, 129.76, 127.35, 127.32 (q, J = 30.7 Hz), 127.20, 126.26, 126.09, 123.71 (q, J = 272.8), 123.67, 122.91, 122.86, 122.79, 122.25, 117.41 (q, J = 5.5 Hz), 67.10, 67.05, 57.87, 54.52. HRMS (ESI) (M+1): 494.1453 calcd for $C_{24}H_{23}ClF_3N_3O_3$ (M+1) = 494.1380.

5.2.5. 1-(3-*tert*-Butyl-1-p-tolyl-1*H*-pyrazol-5-yl)-3-(4-methyl-3-(4-(pyridin-3-yl)pyrimidin-2-ylamino)phenyl)urea (BIRBvec, 8)

To a stirred solution of 100 mg (0.436 mmol, 1.5 equiv) **28** in 5 mL DCM was added 5 mL $NaHCO_3$ and the mixture was cooled to 0 °C in an ice bath. Stirring was stopped and 277 μL (0.523 mmol, 1.5 equiv) of a 20% solution of phosgene in toluene was added directly to the DCM layer via syringe. Stirring was then continued for 4 h. 97 mg amine **12** (0.349 mmol) was then added and the reaction was allowed to proceed for 14 h. The reaction was added to a 250 mL separatory funnel containing water (20 mL) and DCM (100 mL). The organic layer was separated, dried over $MgSO_4$, and then concentrated in vacuo to yield a brown residue that was purified by flash column chromatography on a Biotage Sp1 system (3–8% MeOH/DCM) to yield 143 mg of **8** (0.231 mmol, 66.2% yield) as a white solid, which was dried in a vacuum oven at 60 °C for 6 h.

^{1}H NMR (300 MHz, DMSO-d_6): δ 9.29 (d, 1H, J = 1.6 Hz), 8.95 (s, 1H), 8.90 (s, 1H), 8.85 (s, 1H), 8.69 (dd, 1H, J = 1.6 Hz, J = 4.8 Hz), 8.47–8.52 (m, 2H), 8.31 (s, 1H), 8.29 (s, 1H), 7.82 (d, 1H, J = 1.9 Hz), 7,52 (m, 1H), 7.43 (d, 1H, J = 5.2 Hz), 7.39 (dd, 2H, J = 2.0 Hz, J = 6.5 Hz), 7.35 (d, 2H, J = 6.5 Hz), , 6.38 (s, 1H), 2.37 (s, 3H), 2.19 (s, 3H), 1.26 (s, 9H). ^{13}C NMR (75 MHz, DMSO-d_6): δ 162.39, 161.83, 161.41, 160.33, 152.30, 152.16, 149.02, 138.80, 138.15, 137.70, 136.83, 135.41, 133.05, 131.14, 130.59 (2C), 126.18, 125.30 (2C), 124.70, 115.23, 115.05, 108.48, 79.93, 32.86, 31.06, 21.46, 18.34. HRMS (ESI) (M+1): 533.2772 calcd for $C_{31}H_{32}N_8O$ (M+1) = 533.2699.

5.2.6. 4-(4-(3-(3-*tert*-Butyl-1-*p*-tolyl-1*H*-pyrazol-5-yl)ureido)-phenoxy)-*N*-methylpicolinamide (BIRBavar, 9)

To a stirred solution of 100 mg (0.436 mmol, 1.5 equiv) **28** in 5 mL DCM was added 5 mL $NaHCO_3$ and the mixture was cooled to 0 °C in an ice bath. Stirring was stopped and 277 μL (0.523 mmol, 1.5 equiv) of a 20% solution of phosgene in toluene was added directly to the DCM layer via syringe. Stirring was then continued for 4 h. 98 mg amine **13** (0.349 mmol) was then added and the reaction was allowed to proceed for 14 h. The reaction was added to a 250 mL separatory funnel containing water (20 mL) and DCM (100 mL). The organic layer was separated, dried over $MgSO_4$, and then concentrated in vacuo to yield a yellow solid that was purified by flash column chromatography on a Biotage Sp1 system (1–5% MeOH/DCM) to yield 120 mg of **8** (0.241 mmol, 69.0% yield) of an off white solid, which was dried in a vacuum oven at 60 °C for 6 h.

^{1}H NMR (300 MHz, DMSO-d_6): δ 9.16 (s, 1H), 8.85 (q, 1H, J = 4.8 Hz), 8.52 (d, 1H, J = 5.5 Hz), 8.37 (s, 1H), 7.53 (d, 2H, J = 5.6 Hz), 7.33–7.43 (m, 5H), 7.12–7.16 (m, 3H), 6.37 (s, 1H), 2.79 (d, 3H, J = 4.8 Hz), 2.38 (s, 3H), 1.28 (s, 9H). ^{13}C NMR (75 MHz, DMSO-d_6): δ 166.85, 164.63, 161.39, 153.28, 152.47, 151.21, 148.45, 138.17, 137.94, 137.67, 136.93, 130.57 (2C), 125.24 (2C), 122.35, 120.71, 114.85, 109.52, 96.00, 32.88, 31.08 (3C), 26.86, 21.47. HRMS (ESI) (M+1): 499.2452 calcd for $C_{28}H_{30}N_6O_3$ (M+1) = 499.2379.

5.2.7. *N*-Methyl-4-(4-(3-(4-((4-methylpiperazin-1-yl)methyl)-phenyl)-ureido)phenoxy)picolinamide (Gleevavar-Urea, 10)

A solution of 300 mg (1.072 mmol, 1 equiv) **12** in DCM was stirred under argon at room temperature followed by the addition of 174 mg (1.072 mmol, 1 equiv) CDI. The reaction was stirred for 16 h and then a solution of 176 mg of **21** (0.858 mmol, 0.8 equiv) in 5 mL DCM was added dropwise. The reaction was stirred for an additional 24 h upon which time it was poured into 100 mL DCM and then washed with water and brine. The crude material was purified on an Biotage Sp1 system with a silica gel column that was neutralized with a 1% solution of triethylamine in $CHCl_3$. The column was run with a 1–6% MeOH/$CHCl_3$ gradient that also contained 1% triethylamine and provided 176 mg of **10** (0.371 mmol, 34.6% yield) which was dried in a vacuum oven at 60 °C.

^{1}H NMR (300 MHz, CDCl3): δ 8.39 (d, 1H, J = 5.6 Hz), 8.25 (q, 1H, J = 2.2 Hz), 8.17 (s, 1H), 8.07 (s, 1H), 7.60 (d, 1H, J = 2.5 Hz), 7.19–7.37 (m, 7H), 7.03 (dd, 1H, J = 2.5 Hz, J = 5.6 Hz), 6.94 (d, 2H, J = 7.9 Hz), 3.43 (s, 2H), 3.03 (d, 3H, J = 5.1 Hz), 2.30–2.70 (br m, 8H), 2.29 (s, 3H). ^{13}C NMR (75 MHz, $CDCl_3$-d_6): δ 167.21, 165.67, 153.87, 151.90, 150.34, 148.54, 138.16, 137.50, 132.96 (2C), 130.30, 121.73 (2C), 121.36 (2C), 120.04 (2C), 115.21, 109.35, 62.87, 55.40 (2C), 53.29 (2C), 46.34, 26.85. HRMS (ESI) (M+1): 475.2452 calcd for $C_{26}H_{30}N_6O_3$ (M+1) = 475.2379.

5.2.8. 1-(4-Chloro-3-(trifluoromethyl)phenyl)-3-(4-(2-morpholinoethoxy)-phenyl)urea (Nexa-796-Phe, 11)

150 mg isocyanate **16** (0.677 mmol, 1.0 equiv) was dissolved in 5 mL DCM. A solution of 149 mg amine **26** in DCM was added dropwise to the stirred reaction and was allowed to react for 12 h. The reaction was dissolved in 100 mL DCM and washed with water, washed with brine, and then was dried over $MgSO_4$ and concentrated to yield a crude yellow oil. The yellow oil was purified through flash chromatography on a Biotage Sp1 (2–8% MeOH/DCM) to yield 165 mg of **11** (0.373 mmol, 55.2% yield)

^{1}H NMR (300 MHz, DMSO-d_6): δ 9.01 (s, 1H), 8.65 (s, 1H), 8.10 (d, 1H, J = 2.0 Hz), 7.57–7.61 (m, 2H), 7.35 (d, 2H, J = 9.0 Hz), 6.88

(d, 2H, J = 9.0 Hz), 4.03 (t, 2H, J = 5.7 Hz), 3.57 (m, 4H), 2.66 (t, 2H, J = 5.7 Hz), 2.47 (m, 4H): δ 154.84, 153.41, 140.44, 133.04, 132.79, 127.52 (q, J = 30.5 Hz), 123.73, 123.69 (q, J = 273.0),122.84, 121.36 (2C), 117.44 (q, J = 6.0 Hz), 115.50 (2C), 67.032 (2C), 66.33, 57.94, 54.51 (2C). HRMS (ESI) (M+1): 444.1296 calcd for $C_{20}H_{21}ClF_3N_3O_3$ (M+1) = 444.1224.

5.3. Molecular overlap

Three dimensional crystal structures of Gleevec® bound to C-Abl (2HYY), Nexavar® bound to B-Raf (1UWH), and BIRB-796 bound to p38α (1KV2) were downloaded from Protein Data Bank. Water molecules were removed from each crystal structure and monomers of 1KV2 and 1UWH were aligned with 2HYY using Pymol v1.1 from Delano Scientific.

6. Biological evaluation

6.1. General

All assays utilized assay dilution buffer and Mg/ATP cocktail purchased from Millipore. The assay dilution buffer contained 20 mM MOPS, pH 7.2, 25 mM β-glycerophosphate, 5 mM EGTA, 1 mM Na3VO4, and 1 mM dithiothreitol (Millipore Catalog #20-108). The Mg/ATP cocktail contained 75 mM $MgCl_2$, and 0.5 mM cold ATP in assay dilution buffer (Millipore Catalog #20-113). [gamma-32P) Adenosine-5′-triphosphate (10 μCi/μL) was purchased from Perkin–Elmer and used at 0.8 μCi/rxn. Stock 10 mM drug solutions were made up in DMSO and from that were diluted in a half-log manner in ddH_2O.

6.2. p38α Enzymatic assay

7.5 ng recombinant human full length N-terminal GST-tagged p38α (Invitrogen, PV3304), *Escherichia coli* expression) was preincubated at room temperature for 1 h with 1 μL inhibitor and 4 μL assay dilution buffer. The kinase assay was initiated when 5 μL of a solution containing 200 ng recombinant human full length, N-terminal His-tagged MAPKAP-K2 (sPV3316), 200 μM ATP (0.8 μCi hot ATP), and 30 mM $MgCl_2$ in assay dilution buffer was added. The kinase reaction was allowed to continue at room temperature for 25 min and was then quenched with 5 μL 5X protein denaturing buffer (LDS) solution. Protein was further denatured by heating for 5 min at 70 °C. 10 μL of each reaction was loaded into a 15 well, 4–12% precast NuPage gel (invitrogen) and run at 200 V and upon completion, the front which contained excess hot ATP was cut from the gel and discarded. The gel was then dried and developed onto a phosphor screen which was scanned on a Storm 820 scanner and quantitated from optical densitometry using image quant v5.0. A negative control which contained no active enzyme was used as a negative control and a reaction without inhibitor was used as the positive control. Final compound concentrations were 100 μM, 31.6 μM, 10 μM, 3.16 μM, 1 μM, 316 nM, 100 nM, 31.6 nM, 10 nM, 3.16 nM, 1 nM, 316 pM, and 100 pM.

6.3. B-Raf enzymatic assay

The B-Raf biological assay used the same protocol as p38 except it utilized recombinant Human Full-Length GST-tagged B-Raf (invitrogen, pv3848) and recombinant human full length, N-terminal His-tagged MEK1 (invitrogen, pv3093).

6.4. Abl enzymatic assay

The Abl kinase assay utilized 1 ng/rxn active recombinant mouse Abl, residues 27-1123, containing an N-terminal His6 tag (Millipore, 14-459) and the 100 μM synthetic peptide substrate Abltide (EAIYAAPFAKKK, Millipore, 12-493). Kinase reactions were set up as previously described in the p38 enzymatic assay, however, reactions were quenched with 5 μL 3% phosphoric acid. 10 μL of each reaction was then applied to 2 × 2 cm p81 phosphocellulose squares (Whatmann) and washed a minimum of five times for 5 min with 75 mM phosphoric acid. Squares were then washed with methanol for 2 min and placed in a 24 well Perkin–Elmer plate with 1 mL of scintillation fluid and counted on a Perkin–Elmer Top Count scintillation counter.

Acknowledgment

This research was supported by a grant from the National Foundation for Cancer Research.

References and notes

1. Schiffer, C. A. *N. Eng. J. Med.* **2007**, *357*, 258.
2. Capdeville, R.; Buchdunger, E.; Zimmermann, J.; Matter, A. *Nat. Rev. Drug Disc.* **2002**, *1*, 493.
3. Buchdunger, E.; Matter, A.; Druker, B. J. *Biochim. Biophys. Acta* **2001**, *1551*, M11.
4. Liu, Y.; Gray, N. S. *Nat. Chem. Biol.* **2006**, *2*, 358.
5. Nagar, B. et al *Cancer Res.* **2002**, *62*, 4236.
6. Regan, J. et al *J. Med. Chem.* **2003**, *46*, 4676.
7. Kroe, R. R. et al *J. Med. Chem.* **2003**, *46*, 4669.
8. Sherman, S. I. *Endocrinol. Metab. Clin. North Am.* **2008**, *37*, 511. xi.
9. Gupta-Abramson, V. et al *J. Clin. Oncol.* **2008**, *26*, 4714.
10. So, B. J.; Bekaii-Saab, T.; Bloomston, M. A.; Patel, T. *J. Hematol. Oncol.* **2008**, *1*, 18.
11. Zender, L.; Kubicka, S. *Onkologie* **2008**, *31*, 550.
12. Wilhelm, S. M. et al *Mol. Cancer Ther.* **2008**, *7*, 3129.
13. Shim, J. H.; Park, J. W.; Choi, J. I.; Park, B. J.; Kim, C. M. *J. Cancer Res. Clin. Oncol.* **2009**, *135*, 617–625.
14. Garnett, M. J.; Marais, R. *Cancer Cell* **2004**, *6*, 313.
15. Ishimura, N. et al *Cancer Lett.* **2003**, *199*, 169.
16. Li, N.; Batt, D.; Warmuth, M. *Curr. Opin. Investig. Drugs* **2007**, *8*, 452.
17. Tuveson, D. A.; Weber, B. L.; Herlyn, M. *Cancer Cell* **2003**, *4*, 95.
18. Kumar, R. et al *Clin. Cancer Res.* **2003**, *9*, 3362.
19. Fukushima, T. et al *Oncogene* **2003**, *22*, 6455.
20. Ferrara, N.; Hillan, K. J.; Gerber, H. P.; Novotny, W. *Nat. Rev. Drug Disc.* **2004**, *3*, 391.
21. Ahmad, T.; Eisen, T. *Clin. Cancer Res.* **2004**, *10*, 6388S.
22. Eisen, T. et al *Br. J. Cancer* **2006**, *95*, 581.
23. Pargellis, C. et al *Nat. Struct. Biol.* **2002**, *9*, 268.
24. Schultz, R. M. *Prog. Drug Res.* **2003**, *60*, 59.
25. Lee, J. C. et al *Immunopharmacology* **2000**, *47*, 185.
26. Lee, J. C.; Kassis, S.; Kumar, S.; Badger, A.; Adams, J. L. *Pharmacol. Ther.* **1999**, *82*, 389.
27. Kumar, S.; Boehm, J.; Lee, J. C. *Nat. Rev. Drug Disc.* **2003**, *2*, 717.
28. Adams, J. L.; Badger, A. M.; Kumar, S.; Lee, J. C. *Prog. Med. Chem.* **2001**, *38*, 1.
29. Lee, M. R.; Dominguez, C. *Curr. Med. Chem.* **2005**, *12*, 2979.
30. Sullivan, J. E. et al *Biochemistry* **2005**, *44*, 16475.
31. Namboodiri, H. V. et al *Biochemistry* **2010**, *49*, 3611.
32. Fabian, M. A.; Biggs, W. H., IIIrd; Treiber, D. K.; Atteridge, C. E.; Azimioara, M. D. et al. *Nat Biotechnol* **2005**, *23*, 329–336.
33. Karaman, M. W.; Herrgard, S.; Treiber, D. K.; Gallant, P.; Atteridge, C. E. et al. *Nat Biotechnol* **2008**, *26*, 127–132.
34. Fedorov, O. et al *Proc. Natl. Acad. Sci.* **2007**, *104*, 20523.
35. Bankston, D. et al *Org. Process Res. Dev.* **2002**, *6*, 777.
36. Szakacs, Z. et al *J. Med. Chem.* **2005**, *48*, 249.
37. Lutz, F.; Tietze, F. M. *Eur. J. Org. Chem.* **2006**, *2006*, 2314.
38. Baldwin, I. et al *Bioorg. Med. Chem. Lett.* **2008**, *18*, 5285.
39. Baranska, M. et al *J. Appl. Genet.* **2008**, *49*, 201.